

## Stability regions in time delayed two-area LFC system enhanced by EVs

Ausnain NAVEED<sup>1</sup> , Şahin SÖNMEZ<sup>2,\*</sup> , Saffet AYASUN<sup>3</sup> 

<sup>1</sup>Department of Electrical Engineering, Faculty of Engineering,

The University of Azad Jammu and Kashmir, Muzaffarabad, Pakistan

<sup>2</sup>Department of Electronics and Automation, Yesilyurt Vocational High School,  
Malatya Turgut Özal University, Malatya, Turkey

<sup>3</sup>Department of Electrical and Electronics Engineering, Faculty of Engineering, Gazi University, Ankara, Turkey

Received: 16.04.2021

Accepted/Published Online: 03.09.2021

Final Version: 19.01.2022

**Abstract:** With the extensive usage of open communication networks, time delays have become a great concern in load frequency control (LFC) systems since such inevitable large delays weaken the controller performance and even may lead to instabilities. Electric vehicles (EVs) have a potential tool in the frequency regulation. The integration of a large number of EVs via an aggregator amplifies the adverse effects of time delays on the stability and controller design of LFC systems. This paper investigates the impacts of the EVs aggregator with communication time delay on the stability. Primarily, a graphical method characterizing stability boundary locus is implemented. The approach is based on the stability boundary locus that can be easily determined by equating the real and the imaginary parts of the characteristic equation to zero. For a given time delay, the method computes all the stabilizing proportional-integral (PI) controller gains, which constitutes a stability region in the parameter space of PI controller. The effects of communication delay and participation factor of EVs aggregator on the obtained stability regions is thoroughly examined. Results clearly illustrate that stability regions become smaller as the time delay and participation factor of EVs increase. Finally, the accuracy of region boundaries known as real root boundary and complex root boundary is confirmed by time-domain simulations along with an independent algorithm, quasipolynomial mapping-based root finder (QPmR) algorithm.

**Key words:** Communication delays, electric vehicles, load frequency control, PI controller, stability region

### 1. Introduction

The load frequency control (LFC) systems have been widely used in the control of electrical power systems for many years to provide the balance between load demand and generation in each control area and thus to eliminate deviations in system frequency [1]. The stability and reliability of electrical power systems may get worse due to imbalance or sudden power changes occurring between power generation and load demand during the daily operation of the electrical grid. The imbalance between the power generation and load demand in the interconnected network causes rapid deviations of the nominal frequency and the scheduled power exchanges in the tie-lines between control areas [1]. In recent years, the frequency control problem of the interconnected network has been seen as an important issue in terms of the stability of the power systems due to the increasing environmental concerns, the gradual depletion of fossil resources, and the increased penetration of highly variable renewable energy (RE) power generation [2].

The power balance between the generation and load demand is traditionally maintained by controlling

\*Correspondence: ssonmeztr@gmail.com

the real power output of generators through the primary and secondary control schemes. For last few years, the inclusion of electric vehicles (EVs) via an aggregator into LFC systems has gained much attention [3–8]. Owing to the vehicle-to-grid technology and rapid output power control of the batteries of EVs, EVs have become a potential tool for lessening the sporadic impact of RE sources participating in the frequency regulation. The fast response of EVs provides significant improvement in the LFC system performance. The undesired variations in the frequency can be decreased and consequently the frequency response can be enhanced using EVs as they can be utilized as generators or loads. An aggregator is employed to practically coordinate the participation of EVs in frequency regulation market. Accumulating and managing a group of EVs to provide the frequency regulation standards is the prime task of the aggregator [4, 9, 10]. Additionally, EVs' aggregators transceive information about energy capacities of EVs, their electrical power availability, and charging status to the controller. Therefore, the aggregators rearrange control commands to dispatch the participation of EVs for regulating their output power by automatic generation control.

In power system control, a dedicated or open communication system including fiber-optics, power lines and satellites are used for transferring control signals. The latter is generally chosen due to its lower cost but it causes communication delays. Time delay is a widespread problem in LFC systems because of the following: 1) In smart grids, open communication networks could provide efficient bilateral communication; 2) There exists geographically distributed control area and power sources and 3) The communication network is prone to cyber-attacks causing time delays in control signals [11]. The response time for the control signal by independent system operator (ISO) is imperative in frequency regulation service. Generally, ISO sends a control signal to EVs aggregator every 2-6 seconds. ISOs normally have specific protocols for allowing maximum communication delay to react to the regulation command signals. For example, it is reported that ISO of California permits 4-s delay between aggregator and EVs [12, 13]. Thus, it is important to examine the delay-dependent stability of LFC-EVs system.

Many studies report that for transmission of regulation signal, time delays between ISO and the power plants are less significant [4, 7, 11, 13]. Therefore, this study considers the communication time delay on EVs side only. The main reason of such an assumption is that usually ISOs themselves utilize a communication channel between conventional generators and ISOs and consider the time delay requirements of the communication link on their own. The open communication links between EVs and aggregator can be considered another reason. Communication networks like power line communication (PLC), ZigBee, internet, WiFi etc. are used depending on EVs location. These types of networks cause more significant delays than communication channels deployed between ISOs and conventional generators. Moreover, there may be scheduling delays since the aggregators have to manage EVs regulation as well as their charging/discharging [4, 11, 13]. In [4], the authors have shown that the participation of EVs with communication networks having fast-response adversely affects the frequency regulation and stability of LFC systems in frequency regulation service.

In recent years, various research papers have been published in an effort to examine the delay-dependent stability of LFC systems with or without EVs aggregator. Most of the existing published work focuses on the computation of stability delay margins of the system with a predesigned controller. The stability delay margin is defined as the maximum time delay that guaranties the stability of the LFC systems. These techniques are divided into two main categories: 1) frequency-domain direct methods [5, 7, 14–17] and 2) linear matrix inequalities (LMIs) and Lyapunov stability theory-based time-domain methods [4, 8, 18–20]. These methods are able to efficiently compute stability delay margins for any chosen proportional-integral (PI) controller gains. However, one of the main drawbacks of them is that one needs to determine the delay margin and check the

stability whenever the PI controller gains are changed or retuned, causing time-consuming stability checks. In order to avoid such time-consuming stability checks and thereby to save controller tuning time, it is necessary to determine all possible values of PI controller parameters that ensure the stability for the maxim time delay observed, which can be obtained from the historical data.

In our earlier work reported in [20–23], a graphical method proposed in [24, 25] has been effectively used to obtain stability regions for a specified time delay using stability boundary locus in the PI controller parameters space for single and two-area LFC systems. This method known as stability boundary locus (SBL) determines the stability boundary loci by simply equating real and imaginary parts of the characteristic polynomial to zero [24, 25]. Moreover, the SBL method has been efficiently applied to PI controller design presented in [26] and synthesis of PI controller of a wind turbine [27]. However, reported studies in the literature compute stability regions either for LFC systems without considering EVs or single-area LFC-EVs system. This work extensively examines the stability regions of two-area LFC-EVs system calculated for various delay values. The obtained regions comprise stabilizing controller parameters that assure desired dynamic response of the system and validation of those regions is done by quasipolynomial mapping-based root finder (QPmR) algorithm [28] and time-domain simulations [29]. The main contributions of the study are summarized as follows: i) Identification of stability regions of two-area LFC-EVs system using an analytically elegant method for the first time in the literature, ii) An exhaustive analysis of the impact of time delay and participation factor of EVs aggregator and the power plant.

The remaining article is structured as follows: Section 2 presents the dynamical model of two-area LFC-EVs system with time delays. Section 3 provides the implementation of the SBL method. Section 4 gives stability regions and verification studies while Section 5 concludes the paper.

## 2. Time-delayed LFC-EVs system model

A group of EVs is needed to be integrated to the grid for their practically participation in frequency regulation services. EVs aggregator acts as control center and manages the charge/discharge of each EV. The dynamic model of EV is given as follows [4]:

$$G_{EV,i}(s) = \frac{K_{EV,i}}{1+sT_{EV,i}} \quad (1)$$

For ( $i = 1,2$ ),  $K_{EV,i}$  in the first-order transfer function of (1) represents the gain coefficient of the battery, whereas the time constant of the EVs battery is symbolized by  $T_{EV,i}$ . Figure 1 presents system model of two-area LFC-EVs where  $\tau_{EV1}$  and  $\tau_{EV2}$  represent the communication delays from the controller to the electric vehicles in each control area. Exponential transfer functions of  $e^{-s\tau_{EV1}}$  and  $e^{-s\tau_{EV2}}$  are used to model these delays. A lumped model of all the participating EVs comprising of same delay function and resembling the dynamics of EV is achieved by assuming the time constants  $T_{EV,i}$  and the delays  $\tau_{EV,i}$  ( $i = 1,2$ ) for all the EVs to be equal [4].

The PI type controller is adopted as LFC controller. For ( $i = 1,2$ ),  $\Delta X_{gi}$ ,  $\Delta P_{mi}$ ,  $\Delta P_{gi}$ ,  $\Delta P_{Li}$ ,  $\Delta P_{EV,i}$ , and  $\Delta f_i$  in Figure 1 represent the valve position, mechanical power output, power output of generator, load disturbance, and EVs aggregator power output and deviation of frequency, respectively. Moreover,  $M_i$ ,  $D_i$ ,  $\beta_i$ ,  $R_i$  and  $F_{Pi}$  ( $i = 1,2$ ) are the inertia constant of generator, damping coefficient, frequency bias factor, speed regulation, and fraction of turbine power, respectively, whereas  $T_{gi}$ ,  $T_{ri}$ , and  $T_{ci}$  for ( $i = 1,2$ ) are the time constants of turbine, reheat, and governor. Furthermore,  $K_{Pi}$  and  $K_{Ii}$  denote the proportional controller

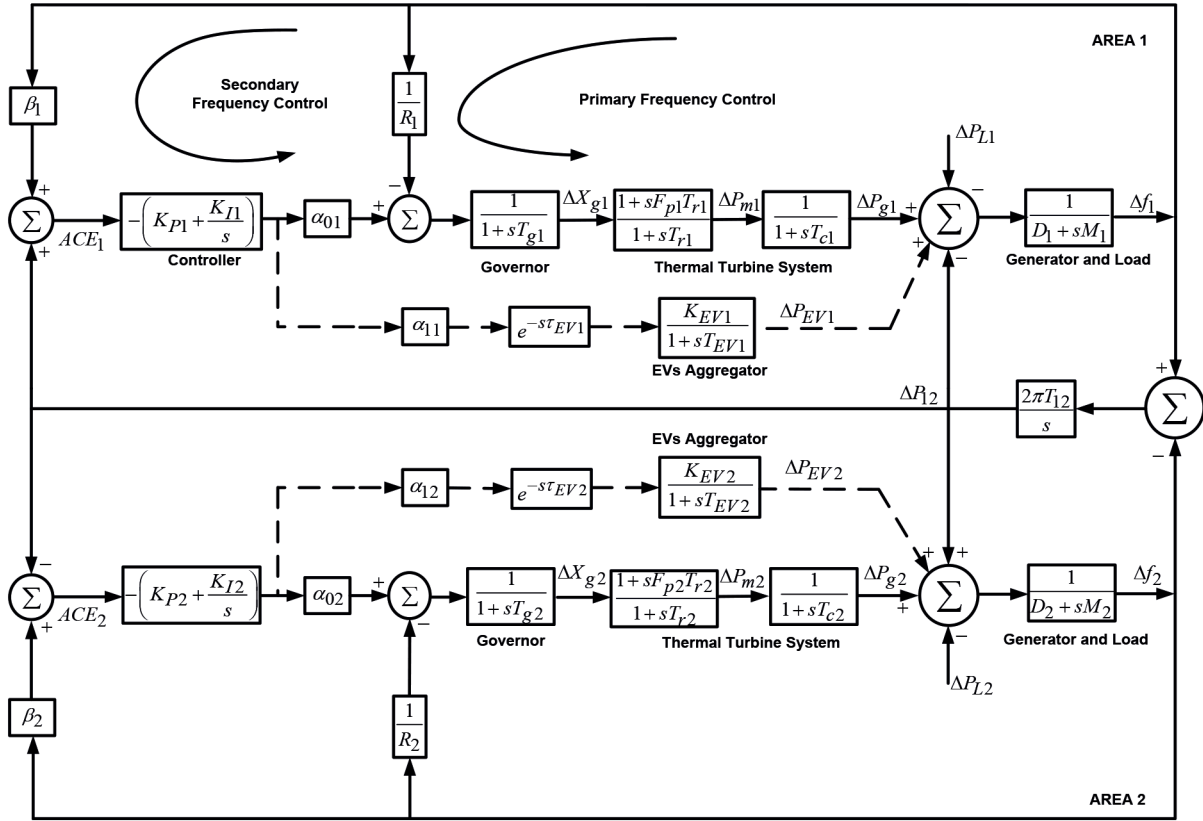


Figure 1. Two-area LFC-EVs system model [4].

gains and integral controller gains of both control areas.

$ACE_i$  for ( $i = 1,2$ ) indicates the area control errors of both areas.  $ACE_1$  is sent to the PI controller as a control signal because of any load changes in area 1. The output signal of the controller is then sent to the generator and EVs based on their participation factors  $\alpha_{01}$  and  $\alpha_{11}$  for regulating the frequency in that area. Likewise, a similar procedure is followed in area 2. The participation ratios of EVs and generators for each area are assumed as  $\alpha_{11}=\alpha_{12}=\alpha_1$  and  $\alpha_{01}=\alpha_{02}=\alpha_0$ , respectively [3]. In Figure 1,  $T_{12}$  expresses the coefficient of tie-line power to enable the scheduling exchange of power in two area LFC system. Based on an assumption that each control area has an identical communication network and thus observe an equal time delay ( $\tau_{EV1} = \tau_{EV2} = \tau$ ) the state-space model of the system shown in Figure 1 can be given as:

$$\begin{aligned} \dot{x}(t) &= A_o x(t) + A_d x(t - \tau) + F \Delta P_L \\ y(t) &= C x(t) \end{aligned} \tag{2}$$

where the inputs and outputs along with the state and output variables are given as:

$$\begin{aligned} x_i(t) &= [ \Delta f_i \quad \Delta P_{gi} \quad \Delta P_{mi} \quad \Delta X_{gi} \quad \Delta P_{EVi} \quad \int ACE_i ], \\ y_i(t) &= [ ACE_i \quad \int ACE_i ], i = 1, 2 \\ x(t) &= [ x_1(t) \quad x_2(t) \quad \Delta P_{12} ]^T, \\ y(t) &= [ y_1(t) \quad y_2(t) ]^T, \\ \Delta P_L &= [ \Delta P_{L1} \quad \Delta P_{L2} ]^T. \end{aligned}$$

The system, input and output matrices,  $A_0$ ,  $A_d$ ,  $F$ , and  $C$  are described in Appendix. In order to define the stability regions, the characteristic polynomial of the two-area LFC-EVs system can simply be computed from (2) as follows:

$$\begin{aligned} \Delta(s, \tau) &= \det[sI - A_o - A_d e^{-\tau s}] = 0 \\ \Delta(s, \tau) &= P(s) + Q(s)e^{-\tau s} + R(s)e^{-2\tau s} = 0 \end{aligned} \tag{3}$$

where  $P(s)$ ,  $Q(s)$ , and  $R(s)$  are the three polynomials in  $s$  having real coefficients in terms of system parameters. The coefficients cannot be presented due to their span. However, the polynomials are stated as follows:

$$\begin{aligned} P(s) &= p_{13}s^{13} + p_{12}s^{12} + p_{11}s^{11} + p_{10}s^{10} + p_9s^9 + p_8s^8 + p_7s^7 + p_6s^6 + p_5s^5 + p_4s^4 \\ &\quad + p_3s^3 + p_2s^2 + p_1s + p_0 \\ Q(s) &= q_{11}s^{11} + q_{10}s^{10} + q_9s^9 + q_8s^8 + q_7s^7 + q_6s^6 + q_5s^5 + q_4s^4 + q_3s^3 + q_2s^2 + q_1s + q_0 \\ R(s) &= r_9s^9 + r_8s^8 + r_7s^7 + r_6s^6 + r_5s^5 + r_4s^4 + r_3s^3 + r_2s^2 + r_1s + r_0 \end{aligned} \tag{4}$$

### 3. Identification of stability regions

This section presents the implementation of the SBL methods into two-area LFC-EVs system whose characteristic equation is given in (3). The proposed stability boundary locus method requires some modifications for the two-area LFC-EVs system as the coefficients of (3) involve some square terms of  $K_P$  and  $K_I$  controller gains [20]. The coefficients of  $P(s)$  polynomial are expressed in terms of PI controller parameters as follows:

$$\begin{aligned} P(s) &= Z_1s^{13} + Z_2s^{12} + Z_3s^{11} + Z_4s^{10} + Z_6s^9 + Z_8s^8 + Z_{10}s^7 + Z_{13}s^6 + Z_{16}s^5 + Z_{19}s^4 + Z_{22}s^3 \\ &\quad + Z_{25}s^2 + K_P Z_5s^{10} + K_P Z_7s^9 + K_I Z_5s^9 + K_P Z_9s^8 + K_I Z_7s^8 + K_P Z_{11}s^7 + K_P^2 Z_{12}s^7 \\ &\quad + K_I Z_9s^7 + K_P Z_{14}s^6 + K_P^2 Z_{15}s^6 + K_I Z_{11}s^6 + 2K_P K_I Z_{12}s^6 + K_P Z_{17}s^5 + K_P^2 Z_{18}s^5 \\ &\quad + K_I Z_{14}s^5 + 2K_P K_I Z_{15}s^5 + K_I^2 Z_{12}s^5 + K_P Z_{20}s^4 + K_P^2 Z_{21}s^4 + K_I Z_{17}s^4 \\ &\quad + 2K_P K_I Z_{18}s^4 + K_I^2 Z_{15}s^4 + K_P Z_{23}s^3 + K_P^2 Z_{24}s^3 + K_I Z_{20}s^3 + 2K_P K_I Z_{21}s^3 \\ &\quad + K_I^2 Z_{18}s^3 + K_P Z_{26}s^2 + K_P^2 Z_{27}s^2 + K_I Z_{23}s^2 + 2K_P K_I Z_{24}s^2 + K_I^2 Z_{21}s^2 \\ &\quad + K_I Z_{26}s + 2K_P K_I Z_{27}s + K_I^2 Z_{24}s + K_I^2 Z_{27} \end{aligned} \tag{5}$$

where  $Z_1s^{13}$  corresponds to the coefficient  $p_{13}s^{13}$ ,  $Z_{25}s^2$  corresponds to the coefficient  $p_2s^2$  excluding  $(K_P, K_I)$  terms,  $Z_{26}s^2$  corresponds to the coefficient  $p_2s^2$  having  $K_P$  terms only,  $Z_{27}s^2$  corresponds to the coefficient  $p_2s^2$  including  $K_P^2$  terms only,  $Z_{23}s^2$  corresponds to the coefficient  $p_2s^2$  having  $K_I$  terms only,  $Z_{24}s^2$  corresponds to the coefficient  $p_2s^2$  including the product term of  $K_P K_I$  and  $Z_{21}s^2$  corresponds to the coefficient  $p_2s^2$  having  $K_I^2$  terms only. All other coefficients are expressed in the same fashion. The simplification of (5) further yields the following form of  $P(s)$  polynomial.

$$\begin{aligned} P(s) &= Z_1s^{13} + Z_2s^{12} + Z_3s^{11} + Z_4s^{10} + Z_6s^9 + Z_8s^8 + Z_{10}s^7 + Z_{13}s^6 + Z_{16}s^5 + Z_{19}s^4 + Z_{22}s^3 + Z_{25}s^2 \\ &\quad + (K_P s + K_I) Z_5s^9 + Z_7s^8 + Z_9s^7 + Z_{11}s^6 + Z_{14}s^5 + Z_{17}s^4 + Z_{20}s^3 + Z_{23}s^2 + Z_{26}s \\ &\quad + (K_P s + K_I)^2 Z_{12}s^5 + Z_{15}s^4 + Z_{18}s^3 + Z_{21}s^2 + Z_{24}s + Z_{27} \end{aligned} \tag{6}$$

After labeling the terms having  $(K_P s + K_I)^2$  as  $Z_b(s)$ , the terms having  $(K_P s + K_I)$  as  $Z_a(s)$  and the terms not containing  $(K_P, K_I)$  as  $C(s)$  in (6),  $P(s)$  polynomial can be expressed in a more simpler form as;

$$P(s) = (K_P s + K_I)^2 Z_b(s) + (K_P s + K_I) Z_a(s) + C(s) \tag{7}$$

Similarly, the coefficients of  $Q(s)$  polynomial are expressed in terms of PI controller parameters as follows:

$$\begin{aligned}
 Q(s) = & K_P Y_1 s^{11} + K_P Y_2 s^{10} + K_I Y_1 s^{10} + K_P Y_3 s^9 + K_I Y_2 s^9 + K_P Y_5 s^8 + K_P^2 Y_4 s^8 + K_I Y_3 s^8 \\
 & + K_P Y_7 s^7 + K_P^2 Y_6 s^7 + K_I Y_5 s^7 + 2K_P K_I Y_4 s^7 + K_P Y_9 s^6 + K_P^2 Y_8 s^6 + K_I Y_7 s^6 \\
 & + 2K_P K_I Y_6 s^6 + K_I^2 Y_4 s^6 + K_P Y_{11} s^5 + K_P^2 Y_{10} s^5 + K_I Y_9 s^5 + 2K_P K_I Y_8 s^5 + K_I^2 Y_6 s^5 \\
 & + K_P Y_{13} s^4 + K_P^2 Y_{12} s^4 + K_I Y_{11} s^4 + 2K_P K_I Y_{10} s^4 + K_I^2 Y_8 s^4 + K_P Y_{15} s^3 \\
 & + K_P^2 Y_{14} s^3 + K_I Y_{13} s^3 + 2K_P K_I Y_{12} s^3 + K_I^2 Y_{10} s^3 + K_P Y_{17} s^2 + K_P^2 Y_{16} s^2 \\
 & + K_I Y_{15} s^2 + 2K_P K_I Y_{14} s^2 + K_I^2 Y_{12} s^2 + K_I Y_{17} s + 2K_P K_I Y_{16} s + K_I^2 Y_{14} s + K_I^2 Y_{16}
 \end{aligned} \tag{8}$$

Similar to the simplification of  $P(s)$  polynomial,  $Q(s)$  polynomial is further simplified to the following form:

$$\begin{aligned}
 Q(s) = & (K_P s + K_I) \left[ Y_1 s^{10} + Y_2 s^9 + Y_3 s^8 + Y_5 s^7 + Y_7 s^6 + Y_9 s^5 + Y_{11} s^4 + Y_{13} s^3 + Y_{15} s^2 + Y_{17} s \right] \\
 & + (K_P s + K_I)^2 \left[ Y_4 s^6 + Y_6 s^5 + Y_8 s^4 + Y_{10} s^3 + Y_{12} s^2 + Y_{14} s + Y_{16} \right]
 \end{aligned} \tag{9}$$

After labeling the terms having  $(K_P s + K_I)^2$  as  $Y_b(s)$  and the terms having  $(K_P s + K_I)$  as  $Y_a(s)$  in (9),  $Q(s)$  polynomial can be expressed in a more simpler form as:

$$Q(s) = (K_P s + K_I)^2 Y_b(s) + (K_P s + K_I) Y_a(s) \tag{10}$$

Likewise, the coefficients of  $R(s)$  polynomial are expressed in terms of PI controller parameters as;

$$\begin{aligned}
 R(s) = & K_P^2 X_1 s^9 + K_P^2 X_2 s^8 + 2K_P K_I X_1 s^8 + K_P^2 X_3 s^7 + K_I^2 X_1 s^7 + 2K_P K_I X_1 s^7 + K_P^2 X_4 s^6 \\
 & + K_I^2 X_2 s^6 + 2K_P K_I X_3 s^6 + K_P^2 X_5 s^5 + K_I^2 X_3 s^5 + 2K_P K_I X_4 s^5 + K_P^2 X_6 s^4 + K_I^2 X_4 s^4 \\
 & + 2K_P K_I X_5 s^4 + K_P^2 X_7 s^3 + K_I^2 X_5 s^3 + 2K_P K_I X_6 s^3 + K_P^2 X_8 s^2 + K_I^2 X_6 s^2 + 2K_P K_I X_7 s^2 \\
 & + K_I^2 X_7 s + 2K_P K_I X_8 s + K_I^2 X_8
 \end{aligned} \tag{11}$$

Similar to  $P(s)$  and  $Q(s)$  polynomials,  $R(s)$  polynomial is rearranged in terms of  $(K_P s + K_I)$  for example,  $X_1 s^7 (K_P s + K_I)^2 = K_P^2 X_1 s^9 + 2K_P K_I X_1 s^8 + K_I^2 X_1 s^7$ . Therefore,

$$\begin{aligned}
 R(s) = & X_1 s^7 (K_P s + K_I)^2 + X_2 s^6 (K_P s + K_I)^2 + X_3 s^5 (K_P s + K_I)^2 + X_4 s^4 (K_P s + K_I)^2 \\
 & + X_5 s^3 (K_P s + K_I)^2 + X_6 s^2 (K_P s + K_I)^2 + X_7 s (K_P s + K_I)^2 + X_8 (K_P s + K_I)^2 \\
 \text{or,} & \\
 R(s) = & (K_P s + K_I)^2 X_1 s^7 + X_2 s^6 + X_3 s^5 + X_4 s^4 + X_5 s^3 + X_6 s^2 + X_7 s + X_8 \\
 \text{or,} & \\
 R(s) = & (K_P s + K_I)^2 X(s)
 \end{aligned} \tag{12}$$

Finally, after substituting the expressions  $P(s)$ ,  $Q(s)$ , and  $R(s)$  in (7), (10), and (12) into the characteristic equation in (3), the following modified equation is obtained.

$$\begin{aligned}
 \Delta(s, \tau) = & P(s) + Q(s)e^{-s\tau} + R(s)e^{-2s\tau} = (K_P s + K_I) Z_a(s) + (K_P s + K_I)^2 Z_b(s) + C(s) \\
 & + \left[ (K_P s + K_I) Y_a(s) + (K_P s + K_I)^2 Y_b(s) \right] e^{-s\tau} + \left[ (K_P s + K_I)^2 X(s) \right] e^{-2s\tau} = 0
 \end{aligned} \tag{13}$$

By denoting  $m = (K_P s + K_I)$ , the characteristic equation in (13) can be expressed in the following form;

$$\begin{aligned}
 \Delta(s, \tau) = & m Z_a(s) + m^2 Z_b(s) + C(s) + \left[ m Y_a(s) + m^2 Y_b(s) \right] e^{-s\tau} + \left[ m^2 X(s) \right] e^{-2s\tau} = 0 \\
 \text{or,} & \\
 \Delta(s, \tau) = & m \left[ Z_a(s) + Y_a(s) e^{-s\tau} \right] + m^2 \left[ Z_b(s) + Y_b(s) e^{-s\tau} + X(s) e^{-2s\tau} \right] + C(s) = 0
 \end{aligned} \tag{14}$$

Setting  $A(s) = [Z_b(s) + Y_b(s)e^{-s\tau} + X(s)e^{-2s\tau}]$  and  $B(s) = [Z_a(s) + Y_a(s)e^{-s\tau}]$  and substituting them into (14) yields the following quadratic form of the characteristic equation:

$$\Delta(s, \tau) = m^2 A(s) + mB(s) + C(s) = 0 \tag{15}$$

The two roots,  $m_1$  and  $m_2$  of (15) can be computed using the following equation;

$$m_{1,2} = (K_P s + K_I) = \frac{-B(s) \pm \sqrt{B(s)^2 - 4A(s)C(s)}}{2A(s)} \tag{16}$$

In order to obtain the stability regions of the two-area LFC-EVs system,  $s = j\omega_c$  when  $\omega_c > 0$  needs to be substituted into the roots given by (16) as;

$$\begin{aligned} (K_P(j\omega_c) + K_I) &= \frac{-B(j\omega_c) \pm \sqrt{B(j\omega_c)^2 - 4A(j\omega_c)C(j\omega_c)}}{2A(j\omega_c)} \\ \text{or} \\ 2A(j\omega_c)(jK_P\omega_c + K_I) + B(j\omega_c) \mp \sqrt{B(j\omega_c)^2 - 4A(j\omega_c)C(j\omega_c)} &= 0 \end{aligned} \tag{17}$$

A set of equations given in (18) is obtained by substituting  $e^{-j\omega_c\tau} = \cos(j\omega_c\tau) - j \sin(j\omega_c\tau)$  into  $A(j\omega_c)$  and  $B(j\omega_c)$  terms in (17) and equating the real part  $\Re\{\}$  and imaginary part  $\Im\{\}$  of the equation to zero:

$$\begin{aligned} K_P L_1(\omega_c) + K_I M_1(\omega_c) + N_1(\omega_c) + j(K_P L_2(\omega_c) + K_I M_2(\omega_c) + N_2(\omega_c)) &= 0 \\ K_P L_1(\omega_c) + K_I M_1(\omega_c) + N_1(\omega_c) &= 0 \\ K_P L_2(\omega_c) + K_I M_2(\omega_c) + N_2(\omega_c) &= 0 \end{aligned} \tag{18}$$

where  $L_1(\omega_c)$  and  $M_1(\omega_c)$  belong to the real part of (18) including  $K_P$  and  $K_I$  terms, respectively. Moreover,  $L_2(\omega_c)$  and  $M_2(\omega_c)$  belong to the imaginary part of (18) including  $K_P$  and  $K_I$  terms, respectively. Moreover,  $N_1(\omega_c)$  and  $N_2(\omega_c)$  belong to the real and imaginary part of (18) neither having  $K_P$  nor  $K_I$  terms. The coefficients of  $L_1(\omega_c)$ ,  $L_2(\omega_c)$ ,  $M_1(\omega_c)$ ,  $M_2(\omega_c)$ ,  $N_1(\omega_c)$ , and  $N_2(\omega_c)$  are not given here due to their span. The set of equations in (18) is then solved for  $(K_P, K_I)$  to identify the complex root boundary (CRB) locus  $\ell(K_P, K_I, \omega_c)$  as:

$$\begin{aligned} K_P &= \frac{M_1(\omega_c)N_2(\omega_c) - M_2(\omega_c)N_1(\omega_c)}{L_1(\omega_c)M_2(\omega_c) - L_2(\omega_c)M_1(\omega_c)} \\ K_I &= \frac{L_2(\omega_c)N_1(\omega_c) - L_1(\omega_c)N_2(\omega_c)}{L_1(\omega_c)M_2(\omega_c) - L_2(\omega_c)M_1(\omega_c)} \end{aligned} \tag{19}$$

In addition to complex roots, some roots of (3) may cross the  $j\omega$ -axis from origin. Equation (18) shows that this type of stability change occurs only for  $K_I = 0$  determining the real root boundary (RRB) locus. Therefore, it can be said that the CRB and RRB loci divide the  $K_P, K_I$ - plane in stable and unstable regions.

#### 4. Results and discussion

The results for stability region in two-area LFC-EVs system and their validation by simulation studies and QPmR algorithm are given in this section. The parameters for each area ( $i = 1,2$ ) are given as [3]:

$$\begin{aligned} M_i &= 8.8, D_i = 1, F_{P_i} = 1/6, R_i = 1/11, \beta_i = 21, T_{12} = 0.1, T_{g_i} = 0.2, T_{c_i} = 0.3, T_{r_i} = 12, \\ T_{EV,i} &= 0.1, K_{EV,i} = 1, (i = 1, 2). \end{aligned}$$

It is evident from (16) that the two-area LFC-EVs system yields two different roots  $m_1$  and  $m_2$  which correspond to two different stability regions. Both stability regions are depicted in Figure 2 for the communication time delay  $\tau_1 = \tau_2 = \tau = 1.0\text{s}$  and the participation ratios of  $\alpha_0 = 0.8, \alpha_1 = 0.2$ . These participation factors imply that 80% of the required control effort is provided by the conventional power plant while 20% is provided by the EVs aggregators. As explained in the previous section, the real axis in Figure 2 where  $K_I = 0$  represents the RRB locus. The CRB of  $m_1$  shown by solid line and the CRB of  $m_2$  represented by dashed line are combined to form a stability region depicted in Figure 3. Note the overall stability region in Figure 3 is the intersection of the two stability regions depicted in Figure 2. The regions enclosed by the CRB and RRB in Figure 2 represent a stability region in the parameter space of the PI controller such that for any chosen PI controller gains, the two-area LFC-EVs system will be stable.

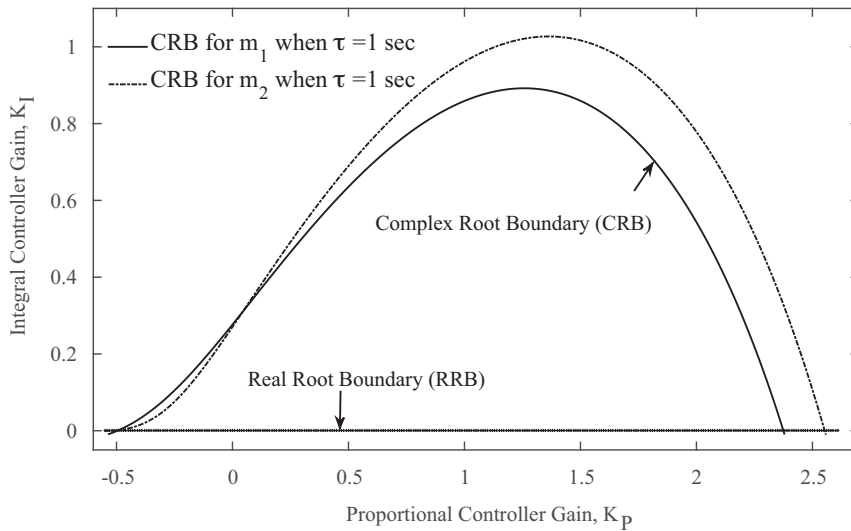


Figure 2. Two stability regions for the selected time delay and participation ratios.

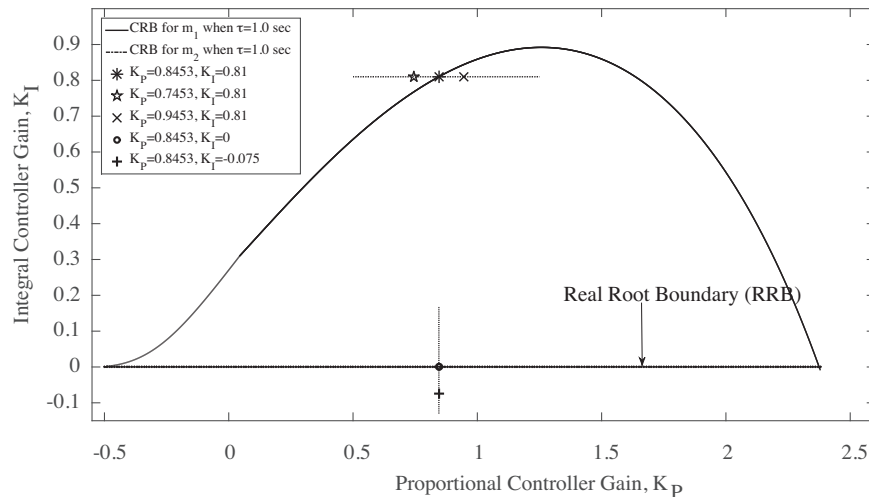


Figure 3. The combined stability region and three test points for the selected time delay and participation ratios.

The stability region with CRB and RRB shown in Figure 3 represents a set of PI controllers that guaranties the stability of the two-area LFC-EVs system for the given communication time delay of  $\tau_1 = \tau_2 = \tau = 1.0s$  and the participation ratios of  $\alpha_0 = 0.8, \alpha_1 = 0.2$ . In order to prove the accuracy of the CRB locus, three different test points are selected by fixing the integral controller gain value at ( $K_I = 0.81$ ) around the CRB locus. As can be seen in Figure 3, these test points include ( $K_P = 0.9453, K_I = 0.81$ ) inside the region labeled as (x) for the stable case, ( $K_P = 0.8453, K_I = 0.81$ ) on the CRB locus labeled as (\*) for the marginally stable case and ( $K_P = 0.7453, K_I = 0.81$ ) outside the region labeled as (★) for the unstable case. The time-domain simulation along with the QPmR algorithm based dominant roots distribution and their zoom picture are shown for ( $K_P = 0.9453, K_I = 0.81$ ) inside the region in Figure 4a. It should be observed that all dominant roots are located in the stable left half of the  $s$ - plane and decaying oscillations in the frequency response depicts the asymptotic stability of the system. Figure 4b shows that the system is marginally stable due to the sustained oscillations in the system frequency response because of the presence of roots on the  $j\omega_c$ - axis for a point ( $K_P = 0.8453, K_I = 0$ ) selected on the CRB locus. However, the system becomes unstable for any controller gains outside the region. This happens because of the presence of a complex roots pair in the unstable right half of the  $s$ -plane. Growing oscillations in the frequency response depicted in Figure 4c also confirm the oscillatory instability of the system for ( $K_P = 0.7453, K_I = 0.81$ ). Similarly, in order to prove the accuracy of the RRB locus, two test points are selected by fixing the proportional controller gain value at ( $K_P = 0.8453$ ) around the CRB locus. As illustrated in Figure 3, two test points are: ( $K_P = 0.8453, K_I = 0$ ) on the RRB locus labeled as (o) for the exponentially stable case and ( $K_P = 0.8453, K_I = -0.075$ ) below the RRB locus labeled as (+) for the unstable case. The distribution of the dominant roots for the selected points around the RRB locus and the frequency responses are depicted in Figure 5. It is clear from Figure 5a that for the PI controller gains of ( $K_P = 0.8453, K_I = 0$ ) on the RRB locus, one of the roots is located at the origin,  $s = 0$  and the remaining roots are in the stable half left plane. The frequency response in Figure 5a clearly indicates that the two-area LFC-EVs system is exponentially stable. On the other hand, for the PI controller gains of ( $K_P = 0.8453, K_I = -0.075$ ), the real root is now in the unstable right half plane and the system is unstable due to the exponentially growing frequency response as shown in Figure 5b.

In the next study, the impact of participation factors of EVs aggregator ( $\alpha_{11} = \alpha_{12} = \alpha_1$ ) in both control areas on the stability region is investigated. For that purpose, three different EVs participation factors are selected, i.e.  $\alpha_1 = 0.1, 0.2$ , and  $0.3$  whereas the time delay is fixed at  $\tau = 1.0s$ . These participation factors imply that 10%, 20%, and 30% of the required control effort are provided by the EVs aggregators with a time delay of  $\tau = 1.0s$ . Figure 6 compares the corresponding stability regions labeled as R1, R2, and R3 for these participation factors. Observe that the largest stability region R1 whose CRB locus is the solid blue line is obtained for  $\alpha_1 = 0.1$ . It should be noted that the stability region gets smaller when the participation factor is increased to  $\alpha_1 = 0.2$ . The stability regions for this case is labeled as R2 and its CRB locus is illustrated by a solid black line in Figure 6. Finally, the stability region labeled as R3 in Figure 6 with a solid red line CRB locus further shrinks for  $\alpha_1 = 0.3$ . Figure 6 clearly illustrates that the size of stability regions decreases as the EVs participation factor increases, whereas the shape of the regions is unchanged. It is evident from Figure 6 that the stability regions get smaller when the contribution of EVs aggregators in frequency regulation rises. This happens due to the presence of communication time delays because the adverse effect of the time delay on the stability region is signified by the increase of the participation ratio of EVs. Finally, regions of R1, R2, and R3 enclosed by the CRB and RRB loci in Figure 6 represents a stability region in the parameter space of the PI controller such that for any chosen PI controller gains, the two-area LFC-EVs system will be stable for the

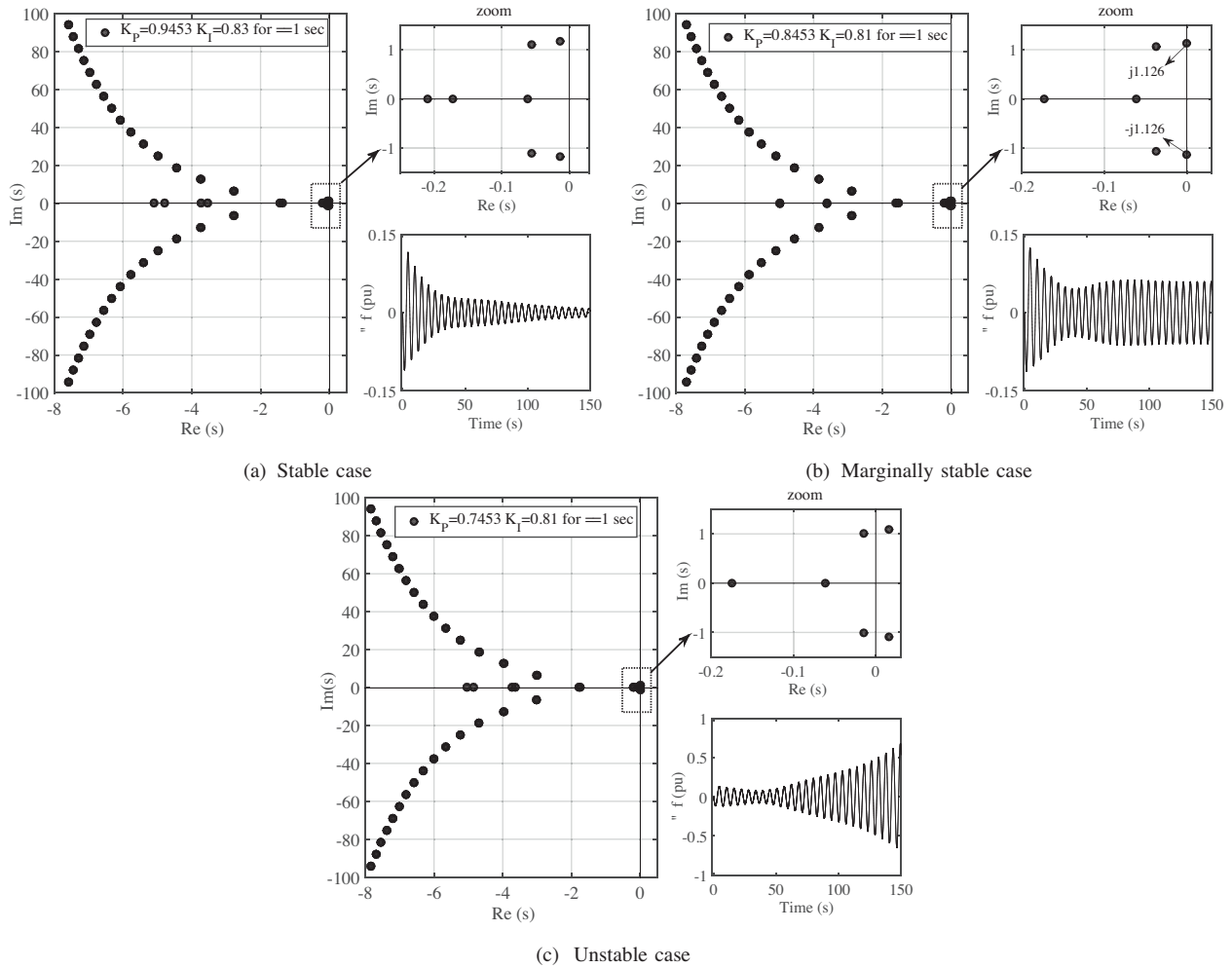


Figure 4. Dominant roots distribution around the CRB and frequency response for the chosen controller gains.

corresponding time delay and the participation factors of EVs.

Finally, the impact of the communication time delay  $\tau$  is investigated for a selected EVs participation factor. Figure 7 illustrates the stability regions, labeled as R1, R2, and R3 for  $\tau = 0.5s, 0.75s,$  and  $1.0s,$  respectively, when the EVs participation factor is chosen as  $\alpha_1 = 0.2$ . Figure 7 clearly shows that the stability regions shrink when the communication delay increases from  $\tau = 0.5s$  to  $\tau = 1.0s,$  whereas their shapes remain unchanged. It must be stated here that RRB locus of stability regions in Figures 6 and 7 is not affected by the participation factor and the time delay since the RRB locus is the x-axis where  $(K_I = 0)$  as explained in the previous section. The stability regions in Figures 6 and 7 clearly illustrate that both EVs participation factor and the time delay associated with EVs aggregator have significant adverse effect on the stability regions.

### 5. Conclusions

This paper has investigated the impact of EVs on the stability region of a two-area LFC system using the stability boundary locus method. For a given time delay and load sharing scheme, stability regions in the parameter space of PI controller are determined. The accuracy of the boundaries of stability region are verified

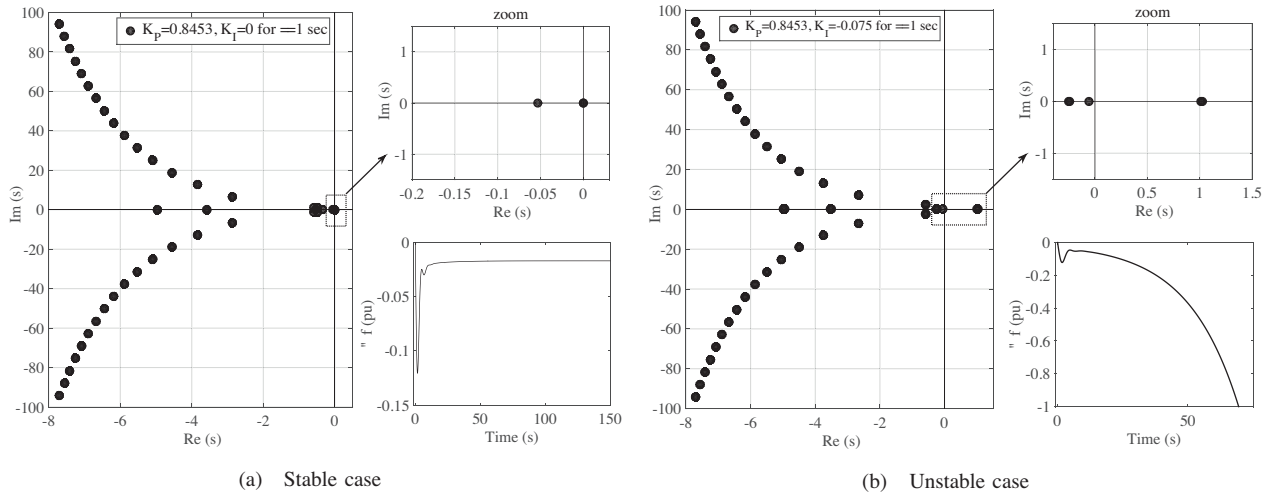


Figure 5. Dominant roots distribution around the RRB and frequency response for the chosen controller gains.

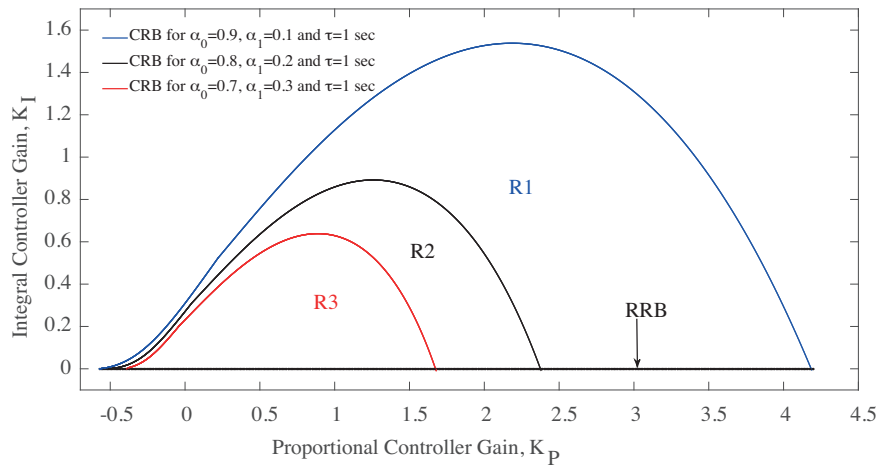
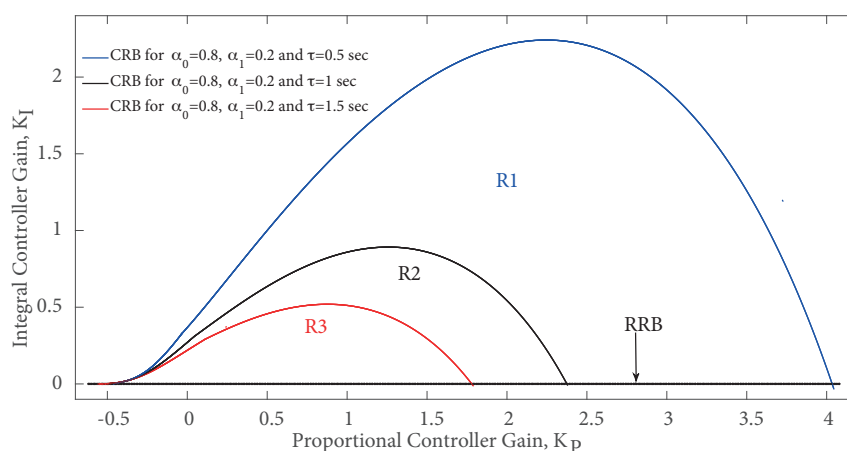


Figure 6. Impact of EVs participation factor on stability regions.

by using time-domain simulations and QPmR algorithm. It has been noticed that size of the stability regions reduces when time delay increases. Moreover, for any given time delay, stability regions become smaller with an increment in participation factor of EVs aggregator. Therefore, it can be concluded that EVs participation along with a time delay can degrade the dynamic performance and cause instability if the PI controller gains and EVs participation factor are not properly selected. It is expected that the results will help us in designing a PI controller that will control the EVs aggregators participating in frequency regulation service. For future studies, robust stability regions assuring the stability of the system for all admissible uncertainties in the participation factors of EVs aggregator will be computed by complex Kharitonov theorem [30]. Moreover, using the rate of change of the frequency (ROCOF), an adaptive scheme will be designed for the selection of the PI controller gains when a dynamic change happens in the participation of EVs.



**Figure 7.** Impact of the time delay on the stability region  $\alpha_0 = 0.8, \alpha_1 = 0.2$ .

### Acknowledgement

The Scientific and Technological Research Council of Turkey (TÜBİTAK) has supported this work under grant number 118E744.

### References

- [1] Kundur P. Power System Stability and Control. New York, NY, USA: McGraw-Hill, 1994.
- [2] Bevrani H, Ghosh A, Ledwich G. Renewable energy sources and frequency regulation: survey and new perspectives. IET Renewable Power Generation 2010; 4 (5): 438-457. doi: 10.1049/iet-rpg.2009.0049
- [3] Janu TNP, Nahavandi S, Hien LV, Trinh H, Wong KP. Static output feedback frequency stabilization of time-delay power systems with coordinated electric vehicles state of charge control. IEEE Transactions on Power Systems 2017; 32 (5): 3862-3874. doi: 10.1109/TPWRS.2016.2633540
- [4] Ko K, Sung DK. The effect of EV aggregators with time-varying delays on the stability of a load frequency control system. IEEE Transactions on Power Systems 2018; 33 (1): 669 – 680. doi: 10.1109/TPWRS.2017.2690915
- [5] Naveed A, Sönmez Ş, Ayasun S. Impact of electric vehicle aggregator with communication time delay on stability regions and stability delay margins in load frequency control system. Journal of Modern Power Systems and Clean Energy 2021; 9 (3): 595-601. doi: 10.35833/MPCE.2019.000244
- [6] Fan H, Jiang L, Zhang CK, Mao C. Frequency regulation of multi-area power systems with plug-in electric vehicles considering communication delays. IET Generation, Transmission & Distribution 2016; 10 (14): 3481-3491. doi: 10.1049/iet-gtd.2016.0108
- [7] Khalil A, Peng AS. Delay margin computation for load frequency control system with plug-in electric vehicles. International Journal of Power and Energy Systems 2018; 38(3): 1-17. doi: 10.2316/Journal.203.2018.3.203-0060
- [8] Zhou SJ, Zeng HB, Xia, HQ. Load frequency stability analysis of time-delayed multi-area power systems with EVs aggregators based on Bessel-Legendre inequality and model reduction technique. IEEE Access 2020; 8: 99948-99955. doi: 10.1109/ACCESS.2020.2997002
- [9] Bessa RJ, Matos MA, Soares FJ. Framework for the participation of EV aggregators in the electricity market,” in: IEEE International Electric Vehicle Conference (IEVC), Florence, Italy; 2014. pp. 1-8.
- [10] Carreira AM, Jorgea HM, Antunesa CH. Energy management systems aggregators: A literature survey. Renewable & Sustainable Energy Reviews 2017; 73: 1160-1172. doi: 10.1016/j.rser.2017.01.179

- [11] Ko K, Sung DK. The Effect of cellular network-based communication delays in an EV aggregator's domain on frequency regulation service. *IEEE Transactions on Smart Grid* 2019; 10 (1): 65-73. doi: 10.1109/TSG.2017.2731846
- [12] Jiang L, Yao W, Wu QH, Wen JY, Cheng SJ. Delay-dependent stability for load frequency control with constant and time-varying delays. *IEEE Transactions on Power Systems* 2012; 27 (2): 932-941. doi: 10.1109/TPWRS.2011.2172821
- [13] Bilh A, Naik K, El-Shatshat R. Evaluating electric vehicles' response time to regulation signals in smart grids. *IEEE Transactions on Industrial Informatics* 2018; 14 (3): 1210-1219. doi: 10.1109/TII.2017.2750638
- [14] Sönmez Ş, Ayasun S, Nwankpa CO. An exact method for computing delay margin for stability of load frequency control systems with constant communication delays. *IEEE Transactions on Power Systems* 2016; 31 (1): 370-377. doi: 10.1109/TPWRS.2015.2403865
- [15] Sönmez Ş, Ayasun S. Gain and phase margins-based delay margin computation of load frequency control systems using Rekasius substitution. *Transactions of the Institute of Measurement and Control* 2019; 41 (12): 3385-3395. doi: 10.1177/0142331219826653
- [16] Naveed A, Sönmez Ş, Ayasun S. Identification of stability delay margin for load frequency control system with electric vehicles aggregator using Rekasius substitution. In: *IEEE 2019 Milan PowerTech*; Milan, Italy; 2019. pp. 1-6.
- [17] Naveed A, Sönmez Ş, Ayasun S. Impact of load sharing schemes on the stability delay margins computed by Rekasius substitution method in load frequency control system with electric vehicles aggregator. *International Transactions on Electrical Energy Systems* 2021; 31(3): 1-18. doi:10.1002/2050-7038.12884
- [18] Jin L, Zhang CK, He Y, Jiang L, Wu M. "Delay-dependent stability analysis of multi-area load frequency control with enhanced accuracy and computation efficiency," *IEEE Transactions on Power Systems* 2019; 34 (5): 3687-3696. doi: 10.1109/TPWRS.2019.2902373
- [19] Hua C, Wang Y. Delay-dependent stability for load frequency control system via linear operator inequality. *IEEE Transactions on Cybernetics* 2020; early access. doi: 10.1109/TCYB.2020.3037113
- [20] Sönmez Ş, Ayasun S. Stability region in the parameter space of PI controller for a single-area load frequency control system with time delay. *IEEE Transactions on Power Systems* 2016; 31 (1): 829-830. doi: 10.1109/TPWRS.2015.2412678
- [21] Sönmez Ş. Computation of stability regions for load frequency control systems including incommensurate time delays. *Turkish Journal of Electrical Engineering and Computer Science* 2019; 27(6): 4596-4607. doi: 10.3906/elk-1904-6
- [22] Naveed A, Sönmez Ş, Ayasun S. Stability Regions in the Parameter Space of PI Controller for LFC System with EVs Aggregator and Incommensurate Time Delays. in: *IEEE 1st Global Power, Energy and Communication Conference (GPECOM)*, Nevsehir, Turkey; 2019. pp. 461-466.
- [23] Sönmez Ş, Ayasun S. Computation of PI controllers ensuring desired gain and phase margins for two-area load frequency control system with communication time delays. *Electric Power Components and Systems* 2018; 46(8): 938-947. doi: 10.1080/15325008.2018.1509914
- [24] Söylemez MT, Munro N, Baki H. Fast calculation of stabilizing PID controllers. *Automatica* 2003; 39(1): 121-126. doi: 10.1016/S0005-1098(02)00180-2
- [25] Tan N, Kaya I, Yeroğlu C, Atherton DP. Computation of stabilizing PI and PID controllers using the stability boundary locus. *Energy Conversion and Management* 2006; 47 (18-19): 3045-3058. doi: 10.1016/j.enconman.2006.03.022
- [26] Hamamci SE, Tan N. Design of PI controllers for achieving time and frequency domain specifications simultaneously. *ISA Transactions* 2006; 45(4): 529-543. doi: 10.1016/S0019-0578(07)60230-4
- [27] Wang J, Tse N, Gao Z. Synthesis on PI-based pitch controller of large wind turbines generator. *Energy Conversion and Management* 2011; 52 (2): 1288-1294. doi: 10.1016/j.enconman.2010.09.026

- [28] Simulink. Simulation and model-based design. Natick, MA, USA: MathWorks, 2019.
- [29] Vyhlídal T, Zítek P. Mapping based algorithm for large-scale computation of quasi-polynomial zeros. *IEEE Transactions on Automatic Control* 2009; 54 (1): 171-177. doi: 10.1109/TAC.2008.2008345
- [30] Sharma J, Hote YV, Prasad R. PID controller design for interval load frequency control system with communication time delay. *Control Engineering Practice* 2019; 89 (8): 154-168. doi: 10.1016/j.conengprac.2019.05.016

**Appendix**

The system matrix along with the input and output matrices of (2) are presented as:

$$A_o = \left[ \begin{array}{c|c|c} [A_{11}]_{6x6} & [A_{12}]_{6x6} & [B_{13}]_{6x1} \\ [A_{21}]_{6x6} & [A_{22}]_{6x6} & [B_{23}]_{6x1} \\ [B_{31}]_{1x6} & [B_{32}]_{1x6} & [B_{33}]_{1x1} \end{array} \right], A_{ij} = \begin{bmatrix} 0_{5x1} & 0_{5x5} \\ 2\pi T_{12} K_{Pi} & 0_{1x5} \end{bmatrix},$$

$$i, j = 1, 2 (i \neq j)$$

$$A_d = \left[ \begin{array}{c|c} [A_{d11}]_{6x6} & [A_{d12}]_{6x7} \\ [A_{d21}]_{7x6} & [A_{d22}]_{7x7} \end{array} \right], A_{d11} = \begin{bmatrix} 0_{4x5} & 0_{4x1} \\ 0_{1x5} & \frac{\alpha_{11} K_{EV1}}{T_{EV1}} \\ 0_{1x5} & 0 \end{bmatrix},$$

$$A_{d22} = \begin{bmatrix} 0_{4x6} & 0_{4x1} \\ 0_{1x6} & \frac{\alpha_{12} K_{EV2}}{T_{EV2}} \\ 0_{2x6} & 0_{2x1} \end{bmatrix}, A_{d12} = [0_{6x7}], A_{d21} = [0_{7x6}] \quad B_{13} = \left[ \begin{array}{ccc} -\frac{1}{M_1} & 0_{1x4} & \frac{K_{P1}\beta_1}{M_1} - K_{I1} \end{array} \right]^T,$$

$$B_{23} = \left[ \begin{array}{ccc} \frac{1}{M_2} & 0_{1x4} & \frac{K_{P2}\beta_2}{M_2} - K_{I2} \end{array} \right]^T,$$

$$B_{31} = -B_{32} = [2\pi T_{12} \quad 0_{1x5}], B_{33} = 0,$$

$$F = \begin{bmatrix} F_1 \\ F_2 \end{bmatrix}^T, F_1 = \left[ \begin{array}{cc} -\frac{1}{M_1} & 0_{1x12} \end{array} \right], F_2 = \left[ \begin{array}{ccc} 0_{1x6} & -\frac{1}{M_2} & 0_{1x6} \end{array} \right],$$

$$C = \begin{bmatrix} C_1 \\ C_2 \end{bmatrix}, C_1 = \begin{bmatrix} 1 & 0_{1x11} & 1 \\ 0_{1x5} & 1 & 0_{1x7} \end{bmatrix}, C_2 = \begin{bmatrix} 0_{1x6} & 1 & 0_{1x4} & 0 & -1 \\ 0_{1x6} & 0 & 0_{1x4} & 1 & 0 \end{bmatrix},$$

$$A_{ii} = \begin{bmatrix} -\frac{D_i}{M_i} & \frac{1}{M_i} & 0 & 0 & \frac{1}{M_i} & 0 \\ 0 & -\frac{1}{T_{ci}} & \frac{1}{T_{ci}} & 0 & 0 & 0 \\ -\frac{F_{Pi}}{T_{gi}R_i} & 0 & -\frac{1}{T_{ri}} \left( \frac{1}{T_{ri}} - \frac{F_{Pi}}{T_{gi}} \right) & 0 & 0 & \frac{\alpha_{0i}F_{Pi}}{T_{gi}} \\ -\frac{1}{T_{gi}R_i} & 0 & 0 & -\frac{1}{T_{gi}} & 0 & \frac{\alpha_{0i}}{T_{gi}} \\ 0 & 0 & 0 & 0 & -\frac{1}{T_{EVi}} & 0 \\ K_{Pi} \left( \frac{\beta_i D_i}{M_i} - 2\pi T_{12} \right) - K_{Ii} \beta_i & -\frac{K_{Pi} \beta_i}{M_i} & 0 & 0 & -\frac{K_{Pi} \beta_i}{M_i} & 0 \end{bmatrix}.$$

$$i = 1, 2.$$